UNIVERSIDAD NACIONAL DE COLOMBIA
SEDE MEDELLÍN
FACULTAD DE MINAS

DYNA
http://dyna.medellin.unal.edu.co/

# Evaluation of coupled porewater pressure and stress-strain constitutive model in granular soils

Oscar Moreno-Torres [a], Gustavo Chang-Nieto [b] & Andrés Salas-Montoya [c]

[a] *Civil Engineering Department, Universidad del Magdalena, Santa Marta, Colombia and Civil Engineering Department, Universidad de la Guajira, Riohacha, Colombia. oshemoreno@yahoo.com*
[b] *Civil Engineering Department, Universidad del Magdalena, Santa Marta, Colombia. gchang@engineer.com*
[c] *Civil Engineering Department, Universidad Nacional de Colombia, Manizales, Colombia, asalasmo@unal.edu.co*

Received: August 19th, 2016. Received in revised form: March 29th, 2017. Accepted: November 25th, 2017.

**Abstract**
The evaluation of performance of three coupled pressure (PWP) generation models and stress-strain constitutive models are applied to granular soils. Those constitutive models are used to recommend them for subsequent application in seismic site-response analysis in effective stresses. The performance of the three-coupled models were evaluated using a database of 25 selected high quality cyclic simple shear tests. The conducted analysis suggested that the simple Coupled GMP and stress-strain constitutive model reasonably capture PWP behavior observed in the laboratory tests, they are analyzed better than using advanced constitutive models, and all of them can be used to perform effective stress-based one-dimensional site-response analysis.

*Keywords*: constitutive models; granular materials; laboratory tests; seismic site-response analysis.

# Evaluación de modelos constitutivos esfuerzo-deformación acoplados con presión de poros en suelos granulares

**Resumen**
En el presente artículo se evaluó el desempeño de tres modelos constitutivos esfuerzo-deformación acoplados con presión de poros a suelos granulares con el objetivo de recomendar su posterior aplicación en el análisis sísmico de respuesta de sitio. El desempeño de los tres modelos acoplados se evaluó utilizando una base de datos de 25 ensayos de corte simple cíclico de alta calidad. Los análisis realizados sugieren que el modelo acoplado de esfuerzo-deformación y GMP captura razonablemente el comportamiento de presión de poros observado en los ensayos de laboratorio de una mejor manera que los modelos constitutivos más avanzados y todos ellos se pueden utilizar para realizar análisis unidimensional de respuesta de sitio considerando esfuerzos efectivos**.**

*Palabras clave*: análisis sísmico de respuesta de sitio; ensayos de laboratorio; materiales granulares; modelos constitutivos,

## 1. Introduction

Seismic site-response analysis is routinely used to quantify the influence of surficial soil layers on ground motion propagation. Typically, one-dimensional (1D) frequency-domain (i.e., equivalent linear) or time-domain (i.e., nonlinear) analyses are performed in a total stress framework. However, downhole array and surface acceleration records available at sites that experienced level-ground cyclic liquefaction—for example, 1964 Niigata (Kawagishi-cho apartment buildings; Ishihara and Koga, 1981); 1987 Superstition Hills (Wildlife site [1])—illustrate that porewater pressure (PWP) generation and concurrent strain-softening can significantly alter the acceleration time histories and response spectra [2]. When these sites are analyzed using a total-stress, equivalent-linear constitutive formulation, poor agreement generally is observed between predicted and field measured response [3-6].

In order to improve the predicted seismic site-response, researchers have proposed PWP generation models (e.g.,

**How to cite:** Moreno-Torres, O., Chang-Nieto, G. and Salas-Montoya, A., Evaluation of coupled porewater pressure and stress-strain constitutive model in granular soils. DYNA, 85(204), pp. 248-256, March, 2018.

Vucetic [4], Matasovic [5], Seed et al. [7], Martin et al. [8], Dobry et al. [9,10], Green et al. [11], Green [12], Polito et al. [13], Ivsic [14]) and effective stress-based soil constitutive models (e.g., Wang et al. [15], Elgamal et al. [16], Park and Byrne [17], Jefferies and Been [18], Boulanger and Ziotopoulou [19]) that can be used for seismic site-response analysis. For example, Booker et al. [20] first proposed an effective stress-based model (named GADFLEA) to study the generation and dissipation of PWP.

In this context, the objective of this study is to evaluate the performance of three coupled PWP and stress-strain constitutive models, used in granular soils, and further recommend them for subsequent application in site-response analysis in effective stresses. For this evaluation, the authors collected 12 bins cyclic simple shear tests (25 individual tests) [21] available in the referred literature. To facilitate comparisons, the laboratory tests were binned based on similar soil response. The PWP coupled stress-strain constitutive models were then evaluated using the laboratory test data, and statistics (i.e., residuals) were used to identify the most effective model.

The three PWP coupled stress-strain constitutive models evaluated corresponded to the:

- Green et al. [11]/Green [12]/Polito et al. [13] model, termed the GMP model coupled with hyperbolic stress-strain model,
- Elgamal model [16], and
- PM4SAND model [19].

## 2. Methodology

In this paper, the authors collected 12 bins cyclic simple shear tests (25 individual tests) [21] available in the referred literature. Those tests were reproduced using three PWP coupled stress-strain constitutive models and the framework of the models used in here is presented next. The results of the numerical simulation were compared with the data obtained in the Laboratory tests. The comparisons with the laboratory tests were evaluated using statistics (i.e., residuals) to identify the most effective model.

### *2.1. Coupled porewater pressure (PWP) and stress-strain constitutive models*

In response to undrained cyclic loading, saturated soils generate excess PWP, which can be separated into transient and residual components. The transient excess PWP results from changes in the mean normal stress during cyclic loading [22,23] and thus do not affect the soil effective stress. The residual excess PWP develops from the tendency for volume decrease during undrained cyclic loading, and therefore result in a decrease in effective stress and stiffness. This residual excess PWP can be defined as the PWP in excess of hydrostatic conditions when the cyclic stress is zero [9,11]. Most PWP generation models were developed to represent residual excess PWP and they can be incorporated in 1D site-response analysis studies to account for changes in effective stress and stiffness related to PWP generation. A brief description of coupled PWP and stress-strain constitutive models is subsequently presented.

#### 2.1.1. GMP model coupled with hyperbolic stress-strain model

Building on the work by Hardin and Drnevich [24], Matasovic [9] proposed two degradation indices that introduce excess PWP-induced material softening into a simplified hyperbolic constitutive model. The modulus degradation index ($\delta_G$) and stress degradation index ($\delta_\tau$) reduce the shear stress mobilized during the loading-unloading process as a result of PWP increase [9], and are defined as:

$$\delta_G = \sqrt{1 - r_u} \qquad \delta_\tau = 1 - (r_u)^{\vartheta} \tag{1}$$

where $r_u$ = excess PWP/$\sigma'_{vo}$ or $\Delta u/\sigma'_{vo}$; and $\vartheta$ = dimensionless exponent generally equal to 3.5 [9] based on matching the stress-strain hysteresis loops over a wide range of $r_u$-values for Santa Monica Beach sand, Wildlife Site sands A and B, Heber Road point bar (PB) and channel fill (CF) sands. The advantage of the degradation indices is that they can use $r_u$ values defined by any PWP generation model.

The modified hyperbolic model presented by Phillips and Hashash [25] was further modified to incorporate the degradation indices previously defined. Moreno-Torres et al. [26] proposed the following equations to compute shear stresses ($\tau$) during loading and unloading-reloading, respectively, corresponding to a given strain.

Loading:

$$\tau = \frac{G_0 \cdot \delta_G \cdot \gamma_c}{1 + \beta' \cdot \left(\frac{\delta_G}{\delta_\tau}\right)^t \cdot \left(\frac{\gamma_c}{\gamma_r}\right)^t} \tag{2}$$

Unloading – Reloading:

$$\tau = F(\gamma_m) \cdot \left[ \frac{G_0 \cdot \delta_G \cdot 2 \cdot \left(\frac{\gamma_c - \gamma_{rev}}{2}\right)}{1 + \beta' \cdot \left(\frac{\delta_G}{\delta_\tau}\right)^t \cdot \left(\frac{\gamma_c - \gamma_{rev}}{2 \cdot \gamma_r}\right)^t} - \frac{G_0 \cdot \delta_G \cdot (\gamma_c - \gamma_{rev})}{1 + \beta' \cdot \left(\frac{\delta_G}{\delta_\tau}\right)^t \cdot \left(\frac{\gamma_m - \gamma_r}{\gamma_r}\right)^t} \right] + \frac{G_0 \cdot \delta_G \cdot (\gamma_c - \gamma_{rev})}{1 + \beta' \cdot \left(\frac{\delta_G}{\delta_\tau}\right)^t \cdot \left(\frac{\gamma_m - \gamma_r}{\gamma_r}\right)^t} + \tau_{rev} \tag{3}$$

where $\gamma_c$ = given shear strain; $\gamma_{rev}$ = reversal shear strain; $\tau_{rev}$ = reversal shear stress; $\gamma_m$ = maximum shear strain; $\gamma_r$ = reference shear strain; t = dimensionless exponent; $\beta'$ = dimensionless factor; $\delta_G$ = modulus degradation index; $\delta_\tau$ = stress degradation index; $F(\gamma_m)$ = reduction factor; and $G_0$ = initial shear modulus.

Based on the energy-based models proposed by Green et al. [11], Green [12], Polito et al. [13], Davis and Berrill [27], [28] and Berrill and Davis [29], proposed the following empirical expression, termed the GMP model:

$$r_u = \sqrt{\frac{W_s}{PEC}} \leq 1 \quad (4)$$

where $W_s$ = energy dissipated per unit volume of soil divided by the initial mean consolidation stress (i.e., normalized unit energy), and PEC = a calibration parameter termed the pseudoenergy capacity. The GMP model was developed using results from stress-controlled, undrained cyTxC tests performed on nonplastic silt-sand mixtures that ranged from clean sands to pure silts. For each test, $W_s$ can be computed as:

$$W_s = \frac{1}{2}\sum_{i=1}^{n-1}(\tau_{i+1} + \tau_i) * (\gamma_{i+1} - \gamma_i) \quad (5)$$

where n = number of load increments imposed during cyclic loading on the stress-strain curve until $r_u = 1$ [11]; $\tau_i$ and $\tau_{i+1}$ = applied shear stress at load increment i and i+1, respectively; and $\gamma_i$ and $\gamma_{i+1}$ = shear strain at load increment i and i+1, respectively. Simply stated, Eq. (4) employs the trapezoidal rule to compute the area bounded by the hysteretic stress-strain loop.

For the GMP model, It is used the model parameter correlations reported by Polito et al. [13], which are defined as:

$$\ln(PEC) = \begin{cases} \exp(0.0139 * D_r) - 1.021 & \text{if } FC < 35\% \\ -0.587 * FC^{0.312} + \exp(0.0139 * D_r) - 1.021 & \text{if } FC \geq \end{cases} \quad (6)$$

where PEC = pseudoenergy capacity; $D_r$ = Relative Density; and FC = fines content.

### 2.1.2. Elgamal model

The numerical framework of this model uses two-phase (fluid and solid) fully-coupled FE (Finite Element) formulation [30,31] based on Biot's theory [32]. The saturated soil system is analyzed such as two-phase material. The *u-p* formulation (displacement of the soil skeleton, *u*, and pore pressure *p* are the primary unknowns) is a simplified numerical framework of this theory [33]. This model was implemented for the simulation of two-dimensional (2D) and 3D response scenarios [30,31,34,35].

The *u-p* formulation is defined by an equation of motion for the solid-fluid mixture, and by an equation of mass conservation for the fluid phase that incorporates equation of motion for the fluid phase and Darcy's law [33]. The two governing equations are presented in the following finite element matrix form [33]:

$$\begin{aligned} &[M]\{\ddot{U}\} + \int_{\Omega} [B]^T\{\sigma'\}\,d\Omega + [Q]\{p\} - \{f^s\} = \{0\} \\ &[Q]^T\{\dot{U}\} + [S]\{\dot{p}\} + [H]\{p\} - \{f^p\} = \{0\} \end{aligned} \quad (7)$$

where [M] is the total mass matrix, $\{\ddot{U}\}$ is the second derivative of displacement vector, $[B]^T$ the strain-displacement transposed matrix, $\{\sigma'\}$ the effective stress tensor, $\Omega$ is the body volume, $d\Omega$ is derivative of the body volume, Q is the discrete gradient operator coupling the solid and fluid phases, $[Q]^T$ is the discrete transposed gradient operator coupling the solid and fluid phases, {p} is the pore pressure vector, [S] is the compressibility matrix, {0} is a cero vector, and [H] is the permeability matrix. The vectors $\{f^s\}$ and $\{f^p\}$ represent the effects of body forces and prescribed boundary conditions for the solid-fluid mixture and the fluid phase, respectively. Those Equations are integrated in the time domain using a single-step predictor multi-corrector scheme of the Newmark type [30,33].

For cyclic and seismic loading scenarios, multi-surface plasticity pressure independent (Von-Mises) and pressure dependent models are able to reproduce the cyclic shear stress-strain response characteristics of the soil conditions. A soil constitutive model pressure-dependent for frictional soils [30,31,34] was developed based on the Prevost [36] original framework. The focus of the formulation was placed on simulating the liquefaction-induced shear strain accumulation mechanism in clean medium-dense sands [31,37]. Special attention was given to the deviatoric-volumetric strain coupling (dilatancy) under cyclic loading, because this causes increased shear stiffness and strength at large cyclic shear strain excursions (i.e., cyclic mobility). The main modeling parameters [38] include standard dynamic soil properties such as low-strain shear modulus and friction angle, as well as parameters to control the dilatancy effects (phase transformation angle, contraction, and dilation), and the level of liquefaction-induced yield strain ($\gamma_y$).

### 2.1.3. PM4SAND model

The sand plasticity model presented follows the basic framework of the stress-ratio controlled, critical state compatible, bounding-surface plasticity model for sand presented by Dafalias and Manzari [39]. The Dafalias and Manzari [39] model extended the previous work by Manzari and Dafalias [40] by adding a fabric-dilatancy related tensor quantity to account for the effect of fabric changes during loading. The fabric-dilatancy related tensor was used to macroscopically model the effect that microscopically observed changes in sand fabric during plastic dilation have on the contractive response upon reversal of loading direction.

*Basic stress and strain terms*

The basic stress and strain terms for the model are described. The basic model is supported on effective stresses and the conventional prime symbol is skipped from the stress terms for convenience. All stresses are effective for the model considered. The stresses are represented by the tensor $\sigma$, the principal effective stresses $\sigma_1$, $\sigma_2$, and $\sigma_3$, the mean effective stress p, the deviatoric stress tensor (s), and the deviatoric stress ratio tensor (r). The implementation was simplified by forming various equations and relationships in terms of the in-plane stresses only. This procedure limits the implementation to plane-strain applications and is not correct for general cases. This has the advantage of simplifying the implementation and improving computational speed by

reducing the number of operations. Expanding the implementation to include the general case should not affect the general features of the model. Consequently, the relationships between the various stress terms can be summarized next:

$$\sigma = \begin{pmatrix} \sigma_{xx} & \sigma_{xy} \\ \sigma_{xy} & \sigma_{yy} \end{pmatrix} \tag{8}$$

$$p = \frac{\sigma_{xx} + \sigma_{yy}}{2} \tag{9}$$

$$s = \sigma - pI = \begin{pmatrix} \sigma_{xx} - p & \sigma_{xy} \\ \sigma_{xy} & \sigma_{yy} - p \end{pmatrix} \tag{10}$$

$$r = \frac{S}{p} = \begin{pmatrix} \frac{\sigma_{xx} - p}{p} & \frac{\sigma_{xy}}{p} \\ \frac{\sigma_{xy}}{p} & \frac{\sigma_{yy} - p}{p} \end{pmatrix} \tag{11}$$

where $\sigma_{xx}$ is the stress in the plane x, $\sigma_{yy}$ is the stress in the plane y, $\sigma_{xy}$ is the shear stress in the plane xy and I is the unitary matrix.

The strain model is represented by a tensor ($\varepsilon$) (strains) that can be separated into the volumetric strain ($\varepsilon_v$) and the deviatoric strain tensor (e). The volumetric strain is represented as:

$$\varepsilon_v = \varepsilon_{xx} + \varepsilon_{yy} \tag{12}$$

where $\varepsilon_{xx}$ is the strain in the plane x, $\varepsilon_{yy}$ is the strains in the plane y and the deviatoric strain tensor (e) is represented by:

$$e = \varepsilon - \frac{\varepsilon_v}{3} I = \begin{pmatrix} \varepsilon_{xx} - \frac{\varepsilon_v}{3} & \varepsilon_{xy} \\ \varepsilon_{xy} & \varepsilon_{xx} - \frac{\varepsilon_v}{3} \end{pmatrix} \tag{13}$$

In incremental form, the deviatoric (de) and volumetric strain ($d\varepsilon_v$) terms are decomposed into an elastic and a plastic part as they are presented next.

$$\begin{aligned} de &= de^{el} + de^{pl} \\ d\varepsilon_v &= d\varepsilon_v^{el} + d\varepsilon_v^{pl} \end{aligned} \tag{14}$$

where $de^{el}$ is the elastic deviatoric strain increment tensor, $de^{pl}$ is the plastic deviatoric strain increment tensor, $d\varepsilon_v^{el}$ is the elastic volumetric strain increment and $d\varepsilon_v^{pl}$ is the plastic volumetric strain increment.

## 3. Results

### *3.1. Prediction of PWP using coupled PWP and stress-strain constitutive models*

The authors used 12 cySS bins for the prediction exercise (Table 1). Model parameters for each of the models were determined using recommendation and formulation for that purpose. Figs. 1 - 3 compare the PWP time histories computed using the GMP model coupled with hyperbolic stress-strain, Elgamal and PM4SAND models to the measured responses of cySS tests in bins S3B, S6B, and S8B, respectively. In general, the GMP model coupled with hyperbolic stress-strain

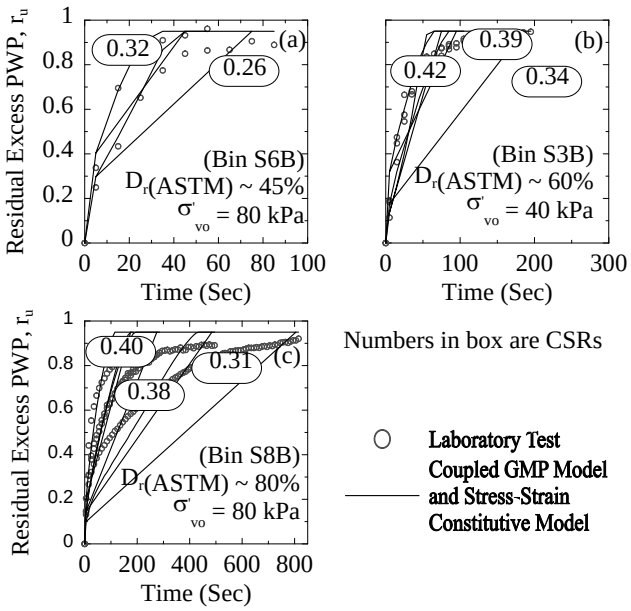


Figure 1. Comparison of calculated GMP model coupled with hyperbolic stress-strain constitutive model and measured PWP ratios for cySS tests: (a) loose specimens; (b) medium-dense specimens; and (c) dense specimens. (Note the differences in the time scales for the various plots.)
Source: The authors.

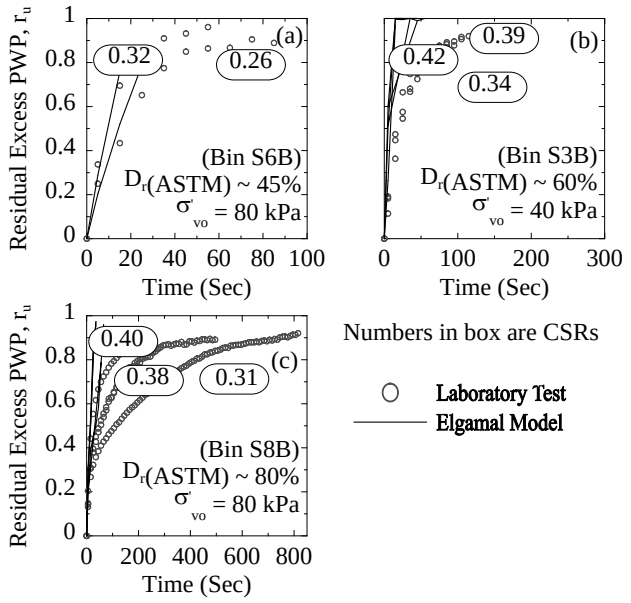


Figure 2. Comparison of calculated Elgamal model and measured PWP ratios for cySS tests: (a) loose specimens; (b) medium-dense specimens; and (c) dense specimens. (Note the differences in the time scales for the various plots.)
Source: The authors.

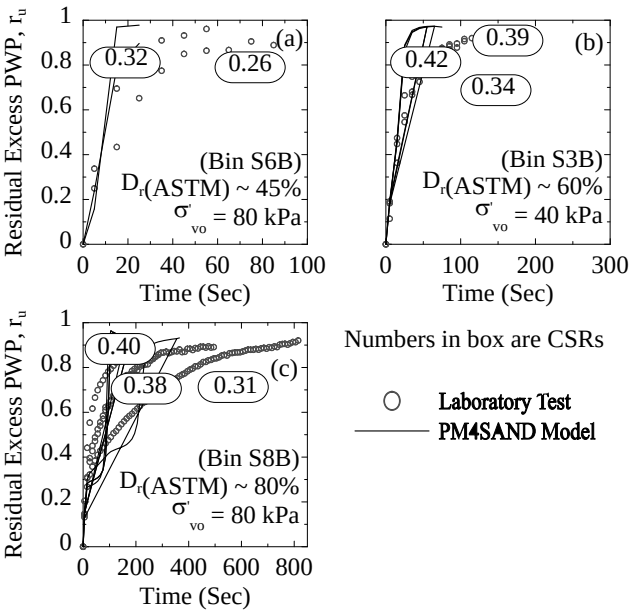


Figure 3. Comparison of calculated PM4SAND model and measured PWP ratios for cySS tests: (a) loose specimens; (b) medium-dense specimens; and (c) dense specimens. (Note the differences in the time scales for the various plots.)
Source: The authors.

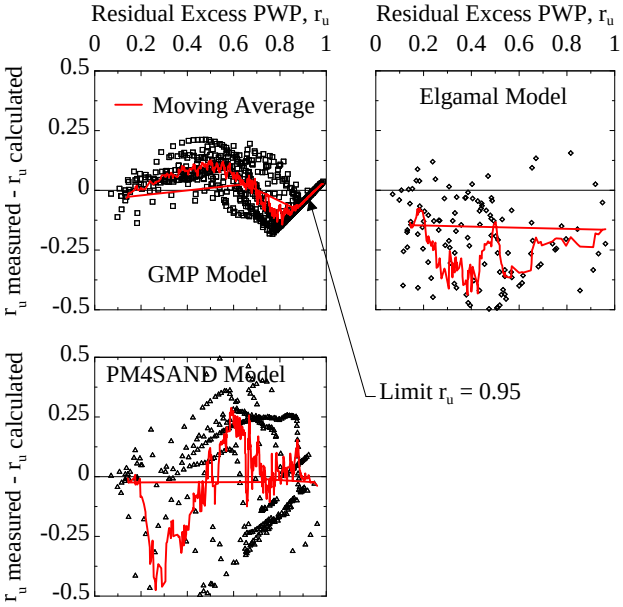


Figure 4. Residuals computed from $r_u$ time histories for tests considered using: (a) GMP model coupled with hyperbolic stress-strain constitutive model; (b) Elgamal model and (c) PM4SAND model.
Source: The authors.

reasonably predict PWP generation in loose to medium-dense specimens (Fig. 1 (a) and (b), respectively). As expected, the model more poorly predict PWP generation in dense specimens (Fig. 1 (c)). The Elgamal and PM4SAND models fairly predict PWP generation in loose to dense specimens (Figs. 2 through 3, respectively) for different CSR magnitudes (i.e., different FSliq).

Table 1.
Summary of cySS tests used in prediction phase of the models.

| Bin | Sub-bin | Test | $e_o$ | $D_{r,c}$ (%) | $\sigma'_c$ (kPa) | CSR | FC (%) | $D_{50}$ (mm) |
|---|---|---|---|---|---|---|---|---|
| S2 | A | M17 | 0.71 | 45 | 40 | 0.170 | 0 | 0.36 |
| | | M72 | 0.71 | 45 | 40 | 0.190 | 0 | 0.36 |
| | | M62 | 0.71 | 45 | 40 | 0.214 | 0 | 0.36 |
| | | M73 | 0.71 | 45 | 40 | 0.225 | 0 | 0.36 |
| | | M82 | 0.71 | 45 | 40 | 0.233 | 0 | 0.36 |
| | B | M47 | 0.71 | 45 | 40 | 0.303 | 0 | 0.36 |
| S3 | A | M61 | 0.67 | 60 | 40 | 0.263 | 0 | 0.36 |
| | | M78 | 0.67 | 60 | 40 | 0.303 | 0 | 0.36 |
| | | M60 | 0.67 | 60 | 40 | 0.292 | 0 | 0.36 |
| | B | M7 | 0.67 | 60 | 40 | 0.347 | 0 | 0.36 |
| | | M66 | 0.67 | 60 | 40 | 0.390 | 0 | 0.36 |
| | | M83 | 0.67 | 60 | 40 | 0.428 | 0 | 0.36 |
| S4 | A | M70 | 0.6 | 80 | 40 | 0.453 | 0 | 0.36 |
| | B | M71 | 0.6 | 80 | 40 | 0.528 | 0 | 0.36 |
| S5 | - | M21 | 0.75 | 35 | 80 | 0.177 | 0 | 0.36 |
| S6 | B | M20 | 0.71 | 45 | 80 | 0.264 | 0 | 0.36 |
| | | M124 | 0.71 | 45 | 80 | 0.328 | 0 | 0.36 |
| S8 | A | M36 | 0.6 | 80 | 80 | 0.241 | 0 | 0.36 |
| | B | M34 | 0.6 | 80 | 80 | 0.310 | 0 | 0.36 |
| | | M105 | 0.6 | 80 | 80 | 0.389 | 0 | 0.36 |
| | | M33 | 0.6 | 80 | 80 | 0.389 | 0 | 0.36 |
| | | M30 | 0.6 | 80 | 80 | 0.401 | 0 | 0.36 |
| S9 | A | M88 | 0.71 | 45 | 180 | 0.163 | 0 | 0.36 |
| | B | M90 | 0.71 | 45 | 180 | 0.192 | 0 | 0.36 |
| | | M103 | 0.71 | 45 | 180 | 0.209 | 0 | 0.36 |

Source: The authors.

Fig. 4 presents the residuals for measured and predicted $r_u$ values (at each cycle) for the 12 cySS bins (25 individual cySS tests) in the prediction dataset. These data illustrate that the coupled GMP with stress-strain constitutive model yields small residuals (±0.25), but contain some bias. The Elgamal and PM4SAND models yield medium residuals (±0.5) with high bias concentrated in the underprediction side for Elgamal model and PM4SAND presents bias in the under and overprediction sides. However, all models qualitatively capture initial liquefaction.

### *3.2. Evaluation of predicted stress-strain behavior using coupled PWP and stress-strain constitutive models*

The authors used the same 12 cySS bins considered for the PWP prediction exercise to evaluate the stress-strain behavior of the models. Model residuals were calculated using computed and measured shear stresses when the measured shear strain, $\gamma_c$ = 0%.

Figs. 5 through 7 compare the stress-strain and excess $r_u$-strain behavior computed using the GMP model coupled with hyperbolic stress-strain, Elgamal and PM4SAND models to the measured responses of cySS tests in bins S3B, S6B, and S8B, respectively. In general, the three models reasonably predict stress-strain and $r_u$-strain behavior in loose to dense specimens for strains less that $\gamma_c$ = 5%. As expected, the coupled GMP model with stress-strain constitutive model more poorly predict stress-strain and $r_u$-strain behavior when dilation becomes more pronounced ($\gamma_c$ > 5% and $r_u$ > 0.65) and significant modulus degradation occurs. Instead, Elgamal and PM4SAND can capture the initial part of dilation spikes and the degradation of the modulus in a good manner when $\gamma_c$ > 5% and $r_u$ > 0.65, but the both codes are not able to support

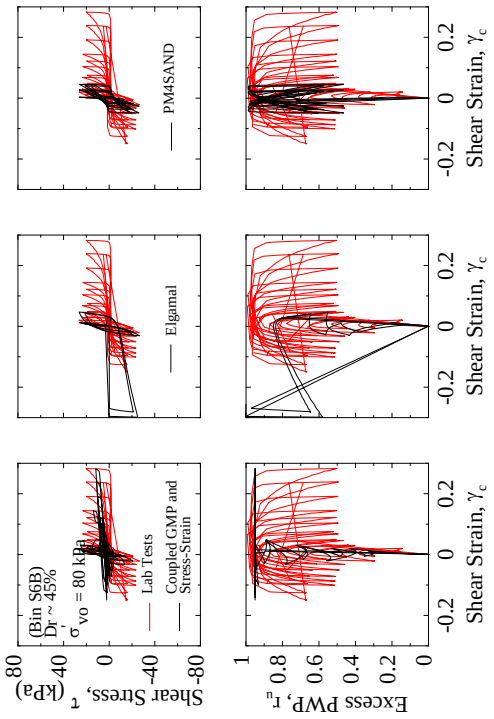


Figure 5. Comparison of calculated GMP coupled with hyperbolic stress-strain, Elgamal and PM4SAND models and measured PWP ratios for cySS test loose specimens.
Source: The authors.

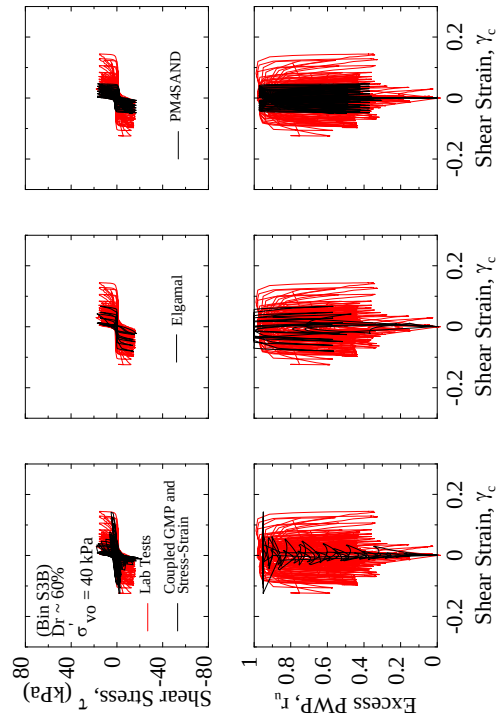


Figure 6. Comparison of calculated GMP coupled with hyperbolic stress-strain, Elgamal and PM4SAND models and measured PWP ratios for cySS test medium-dense specimens.
Source: The authors.

more than a couple of cycles after $r_u > 0.98$ and the codes stop the calculation.

Figs. 5 through 7 compare the stress-strain and excess $r_u$-strain behavior computed using the GMP model coupled with hyperbolic stress-strain, Elgamal and PM4SAND models to the measured responses of cySS tests in bins S3B, S6B, and S8B, respectively. In general, the three models reasonably predict stress-strain and $r_u$-strain behavior in loose to dense specimens for strains less that $\gamma_c = 5\%$. As expected, the coupled GMP model with stress-strain constitutive model more poorly predict stress-strain and $r_u$-strain behavior when dilation becomes more pronounced ($\gamma_c > 5\%$ and $r_u > 0.65$) and significant modulus degradation occurs. Instead, Elgamal and PM4SAND can capture the initial part of dilation spikes and the degradation of the modulus in a good manner when $\gamma_c > 5\%$ and $r_u > 0.65$, but the both codes are not able to support more than a couple of cycles after $r_u > 0.98$ and the codes stop the calculation.

Fig. 8 presents the residuals determined for measured and predicted $\tau/\sigma'_{vo}$ values (CSRs) at each cycle for the 12 cySS bins (25 individual cySS tests) in the prediction dataset. These data illustrate that the coupled GMP with stress-strain constitutive model and PM4SAND yield relatively low residuals (< ±0.25) for $r_u < 0.65$ although the models generally overestimate the values of $r_u$. For high $r_u$-values ($r_u > 0.65$), the residual increases (±0.35), although the bias decreases for both models. Instead, Elgamal model yields very low residuals (< ±0.05) through all $r_u$-values, and no bias is presented with means that this model can reproduce the strain-stress behavior in a good shape.

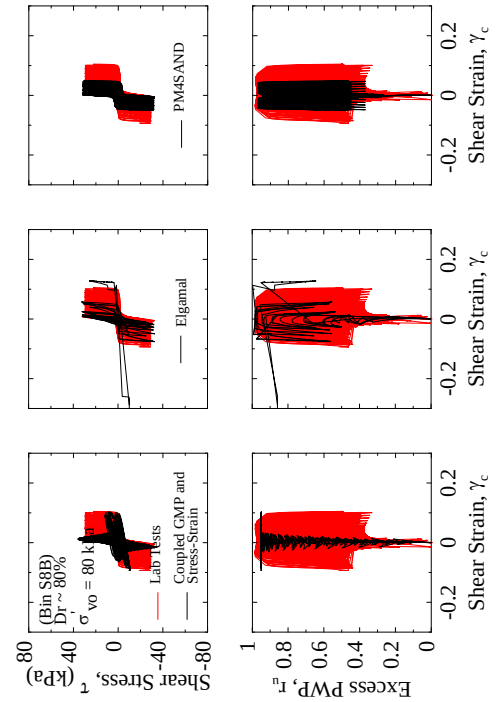


Figure 7. Comparison of calculated GMP coupled with hyperbolic stress-strain, Elgamal and PM4SAND models and measured PWP ratios for cySS test dense specimens.
Source: The authors.

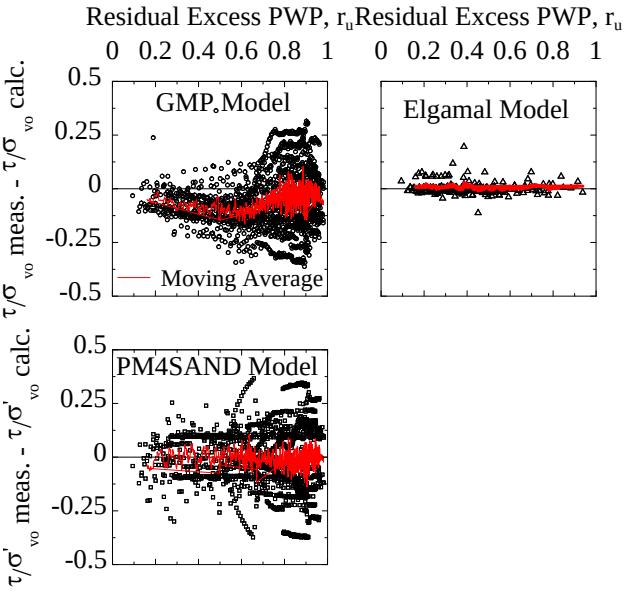


Figure 8. Residuals computed from measured and computed CSR values ($\tau/\sigma'_{vo}$) for tests considered using: (a) GMP model coupled with hyperbolic stress-strain constitutive model; (b) Elgamal model and (c) PM4SAND model..
Source: The authors.

## 4. Conclusion

In this paper, three coupled PWP and stress-strain constitutive models (termed GMP, Elgamal and PM4SAND) are described. Those constitutive model uses different approach to incorporate porewater pressures (PWP) predicted by PWP generation models available in the literature. The evaluation process consisted of a prediction phase, the coupled GMP and stress-strain constitutive model exhibited relatively low residuals compared with Elgamal and PM4SAND model (more advanced constitutive models), but the bias in the coupled GMP and stress-strain constitutive model is more reduced than the other models considered here.

Given the ability of the coupled GMP and stress-strain constitutive model to reasonably predict PWP generation in the prediction phase over the widest range of $r_u$ and over all values of $D_r$, it was expected a reasonable stress-strain prediction. The modified hyperbolic constitutive model coupled with the GMP model qualitatively captures the stress-strain behavior for $r_u \leq 0.65$, but the inability of the hyperbolic constitutive model to reproduce dilation at $r_u$ values exceeding approximately 0.65 reduces the accuracy of the coupled GMP and stress-strain model compared with the Elgamal and PM4SAND models can reproduce the dilation process in better way. The advanced models predict PWP fairly reasonably until initial liquefaction with bias more pronounced. Even, the found limitations that were exposed, all the models can be used in site response analysis with good results in reproduction of the soil response in an earthquake event when liquefaction is an issue.

## 5. List of Symbols

{0} = cero vector
β' = dimensionless factor
$[B]^T$ = strain-displacement transposed matrix
cySS = cyclic simple shear
$D_r$ = relative density
e = deviatoric strain tensor
ε = strains tensor
$\varepsilon_{xx}$ = strain in the plane x
$\varepsilon_{yy}$ = strains in the plane y
$\varepsilon_v$ = volumetric strain
$\delta_G$ = modulus degradation index
$\delta_\tau$ = stress degradation index
de = deviatoric strain
$d\varepsilon_v$ = volumetric strain
$de^{el}$ = elastic deviatoric strain increment tensor
$de^{pl}$ = plastic deviatoric strain increment tensor
$\varepsilon_v^{el}$ = elastic volumetric strain increment
$d\varepsilon_v^{pl}$ = plastic volumetric strain increment.
dΩ = derivative of the body volume
Δu = excess of porewater pressure
FC = fine content
$F(\gamma_m)$ = reduction factor
$\{f^s\}$ = effects of body forces vector
$\{f^p\}$ = prescribed boundary conditions for the solid-fluid mixture and the fluid phase vector
$G_0$ = initial shear modulus
[H] = permeability matrix
I = unitary matrix
$\gamma_c$ = cyclic shear strain
$\gamma_i$ = shear strain at load increment i
$\gamma_{i+1}$ = shear strain at load increment i+1
$\gamma_m$ = maximum shear strain;
$\gamma_r$ = reference shear strain
$\gamma_{rev}$ = reversal shear strain
[M] = total mass matrix
n = number of load increments imposed during cyclic loading on the stress-strain curve
ϑ = dimensionless exponent
Ω is the body volume
p = mean effective stress
PEC = a calibration parameter termed the pseudoenergy capacity
PWP = porewater pressure
{p} = pore pressure vector,
Q = discrete gradient operator coupling the solid and fluid phases,
$[Q]^T$ = discrete transposed gradient operator coupling the solid and fluid phases,
$r_u$ = excess PWP ratio
s = deviatoric stress tensor
[S] = compressibility matrix
σ = The stress tensor
$\sigma_{xx}$ = stress in the plane x
$\sigma_{yy}$ = stress in the plane y
$\sigma_{xy}$ = shear stress in the plane xy
$\{\sigma'\}$ = effective stress tensor
$\sigma'_{vo}$ = initial effective vertical stress
$W_s$ = energy dissipated per unit volume of soil
t = dimensionless exponent
τ = shear stress
$\tau_i$ = applied shear stress at load increment i
$\tau_{i+1}$ = applied shear stress at load increment i+1
$\tau_{rev}$ = reversal shear stress

{Ü} = second derivative of displacement vector

## Acknowledgments

The authors want to thank Dr. Jiaer Wu for sharing his cySS tests with the authors. The authors also thank the Universidad del Magdalena, Universidad de la Guajira and Universidad Nacional de Colombia Sede Manizales for providing the conditions required by authors to further explore and analyze the soils database to be able to complete this study.

## References

[1] Bennett, M.J., McLaughlin, P.V., Sarmiento, J.R. and Youd, T.L., Geotechnical investigation of liquefaction sites, Imperial Valley, California, Open File Report 84-252, U.S Geological Survey, Menlo Park, CA, 1984.

[2] Moroni, M., Sarrazin, M., Venegas, B. and Villarroel, J., Behavior of Chilean bridges with seismic protection devices., Revista de la Construccion, 14(1), pp. 53-59, 2015. DOI: 10.4067/S0718-915X2015000100007.

[3] Lee, K.L. and Finn, A., Earthquake induced settlements in saturated sands., Journal of Geotechnical Engineering, ASCE, 100(GT4), pp. 387-406, 1978.

[4] Vucetic, M., Pore pressure buildup and liquefaction at level sandy sites during earthquakes, Rensselaer Polytechnic Institute, Troy, NY, 1986.

[5] Matasovic, N., Seismic response of composite horizontally-layered soil deposits, University of California, Los Angeles, CA, 1993.

[6] Youd, T.L. and Carter, B., Influence of soil softening and liquefaction on response spectra for bridge design, Report No UT-03.07, Utah Department of Transportation Research and Development Division, USA, 2003.

[7] Seed, H.B., Martin, P.P. and Lysmer, J., The generation and dissipation of pore water pressure during soil liquefaction, Report No EERC-75-26, University of California, Berkeley, California, USA, 1975.

[8] Martin, G.R., Finn, W.D.L. and Seed, H.B., Fundamentals of liquefaction under cyclic loading, J. Geotech. Engrg. Div., 101(5), pp. 423-438, 1975.

[9] Dobry, R., Ladd, R.S., Yokel, F.Y., Chung, R.M. and Powell, D., Prediction of pore water pressure buildup and liquefaction of sands during earthquakes by the cyclic strain method., Building Science Series 183, National Bureau of Standards, U.S. Department of Commerce Washington D.C., USA, 1982.

[10] Dobry, R., Pierce, W.G., Dyvik, R., Thomas, G.E. and Ladd, R.S., Pore pressure model for cyclic straining of sand., Research Report, Rensselaer Polytechnic Institute, Troy, NY, USA, 1985.

[11] Green, R.A., Mitchell, J.K. and Polito, C.P., An energy-based excess pore pressure generation model for cohesionless soils, Proceedings of the John Booker Memorial Symposium, Sidney Australia, A.A Balkema Publishers, Rotterdam, Netherlands, 2000.

[12] Green, R.A., Energy-based evaluation and remediation of liquefiable Soil., Virginia Polytechnic Institute and State University, 2001.

[13] Polito, C.P., Green, R.A. and Lee, J., Pore pressure generation models for sands and silty soils subjected to cyclic loading., Journal of Geotechnical and Geoenvironmental Engineering, 134(10), pp. 1490-1500, 2008. DOI: 10.1061/(ASCE)1090-0241(2008)134:10(1490), 1490-1500.

[14] Ivsic, T., A model for presentation of seismic pore water pressures, Soil Dynamic and Earthquake Engineering, 26, pp. 191-199, 2006. DOI: 10.1016/j.soildyn.2004.11.025.

[15] Wang, Z.L., Chang, C.Y. and Mok, C.M., Evaluation of site response using downhole array data from a liquefied site, Proceedings: 4th International Conference on Recent Advances in Geotechnical Earthquake Engineering and Soil Dynamics and Symposium in Honor of Professor W.D. Liamn Finn, San Diego, California, USA, 2001.

[16] Elgamal, A., Yang, Z. and Parra, E., Computational modeling of cyclic mobility and post-liquefaction site response., Soil Dynamic and Earthquake Engineering 22(2), pp. 259-271, 2002. DOI: 10.1016/S0267-7261(02)00022-2

[17] Park, S.S. and Byrne, P.M., Numerical modelling of soil liquefaction at slope site, fundamentals of soil dynamics, Proceedings of the International Conference on Cyclic Behavior of Soils and Liquefaction, pp. 571- 580, 2004.

[18] Jefferies, M. and Been, K., Soil liquefaction - A critical state approach, Taylor & Francis, New York, 2006.

[19] Boulanger, R.W. and Ziotopoulou, K., PM4Sand (Version 3): A sand plasticity model for earthquake engineering applications, Report No. UCD/CGM-15/01, Center for Geotechnical Modeling, University of California, Davis, CA, USA, 2015.

[20] Booker, J.R., Rahman, M.S. and Seed, H.B., GADFLEA - A computer program for the analysis of pore pressure generation and dissipation during cyclic or earthquake loading, Rep. No. EERC 76-24, Earthquake Engineering Research Center, Univ. of California at Berkeley, Berkeley, California, USA, 1976.

[21] Wu, J., Seed, R.B. and Pestana, J.M., Liquefaction triggering and post liquefaction deformations of Monterey 0/30 sand under uni-directional cyclic simple shear loading, Berkeley, College of Engineering University of California, Berkeley, 2003.

[22] Lambe, T.W. and Whitman, R.V., Soil mechanics, New York, New York, Wiley & Sons, 1969.

[23] Scott, R.F., Principles of soil mechanics, New York, Addison-Wesley Pub, 1963.

[24] Hardin, B.O. and Drnevich, V.P., Shear modulus and damping in soils: Measurement and parameter effects, Journal of Soil Mech. and Found. Eng. Div., 98(SM6), pp. 603-624, 1972.

[25] Phillips, C. and Hashash, Y.M.A., Damping formulation for nonlinear 1D site response analysis., Soil Dynamics and Earthquake Engineering, 29(6), pp. 1143-1158, 2009. DOI: 10.1016/j.soildyn.2009.01.004.

[26] Moreno-Torres, O., Olson, S.M. and Hashash, Y.M.A., A simplified coupled soil-pore water pressure generation for use in site response analysis, Geoflorida 2010, Conference (ASCE) GSP 199, Advances in Analysis, Modeling and Design, West Palm Beach, USA, pp. 3080-3089, 2010. DOI: 10.1061/41095(365)314.

[27] Davis, R.O. and Berrill, J.B., Energy dissipation and seismic liquefaction in sands., Soil Dynamics and Earthquake Engineering, 10(1), pp. 59-68, 1982.

[28] Davis, R.O. and Berrill, J.B., Pore pressure and dissipated energy in earthquakes-field verification., Journal of Geotechnical and Geoenvironmental Engineering, 127(3), pp. 269-274, 1985. DOI: 10.1061/(ASCE)1090-0241(2001)127:3(269),269-274.

[29] Berrill, J.B. and Davis, R.O., Energy dissipation and seismic liquefaction of sands: revised model, Soils Foundation, 25(2), pp. 106-118, 1985. DOI: 10.3208/sandf1972.25.2_106.

[30] Parra, E., Numerical modeling of liquefaction and lateral ground deformation including cyclic mobility and dilation response in soil systems, Rensselaer Polytechnic Institute, Troy, NY, USA, 1996.

[31] Yang, Z. and Elgamal, A., Influence of permeability on liquefaction-induced shear deformation., Journal of Engineering Mechanics, ASCE, 128(7), pp. 720-729, 2002. DOI: 10.1061/(ASCE)0733-9399(2002)128:7(720).

[32] Biot, M.A., The mechanics of deformation and acoustic propagation in porous media., Journal of Applied Physics, 33(4), pp. 1482-1498, 1962. DOI: 10.1063/1.1728759.

[33] Chan, A.H.C., A unified finite element solution to static and dynamic problems in geomechanics., University College of Swansea, Swansea, U.K., 1988.

[34] Yang, Z., Development of geotechnical capabilities into OpenSees platform and their applications in soil-foundation-structure interaction analyses., University of California, Davis, CA, USA, 2002.

[35] Lu, J., Parallel finite element modeling of earthquake site response and liquefaction., University of California, La Jolla, CA, USA, 2006.

[36] Prevost, J.H., A simple plasticity theory for frictional cohesionless soils., International Journal of Soil Dynamics and Earthquake Engineering, 4(1), pp. 9-17, 1985. DOI: 10.1016/0261-7277(85)90030-0.

[37] Elgamal, A., Yang, Z., Parra, E. and Ragheb, A., Modeling of cyclic mobility in saturated cohesionless soils, International Journal of Plasticity, 19(6), pp. 883-905, 2003. DOI: 10.1016/S0749-6419(02)00010-4.
[38] Yang, Z., Elgamal, A. and Parra, E., A computational model for cyclic mobility and associated shear deformation., Journal of Geotechnical and Geoenvironmental Engineering, ASCE, 129(12), pp. 1119-1127, 2003. DOI: 10.1061/(ASCE)1090-0241(2003)129:12(1119).
[39] Dafalias, Y.F. and Manzari, M.T., Simple plasticity sand model accounting for fabric change effects, Journal of Engineering Mechanics, ASCE, 130(6), pp. 622-634, 2004. DOI: 10.1061/(ASCE)0733-9399(2004)130:6(622).
[40] Manzari, M.T. and Dafalias, Y.F., A critical state two-surface plasticity model for sand, Géotechnique, 47(2), pp. 255-272, 1997. DOI: 10.1680/geot.1997.47.2.255.

**O. Moreno-Torres,** received the BSc. Eng in Civil Engineering in 1996, the MSc. degree in Civil Engineering in 2000, and currently PhD Candidate in Civil Engineering. He is an assistant professor in the Civil Engineering Department, Universidad del Magdalena, Colombia and Professor in the Civil Engineering Department, Universidad de la Guajira, Colombia. His research interests include: simulation, modeling and forecasting in geotechnical earthquake engineering.
ORCID: 0000-0003-2038-0824.

**G. Chang-Nieto,** received the BSc. Eng in Civil Engineering in 1997, the MSc. degree in Civil Engineering in 1999, He is an associate professor in the Civil Engineering Department, Universidad del Magdalena, Colombia. His research interests include: simulation, modeling and forecasting in structural earthquake engineering.
ORCID: 0000-0001-8646-708X.

**A. Salas-Montoya,** received the BSc. In Civil Engineering, Universidad del Valle in Cali, Colombia. He is a Dr. in Materials Engineering at Universidad del Valle, Colombia. He had a Posdoctoral position at the Civil and Environmental Engineering Department at the University of Illinois, USA. He is an associate professor at the Universidad Nacional de Colombia at the Civil Engineering Department. He is a researcher in supplementary cementing materials, concrete durability, environmentally friendly materials and sustainability.
ORCID: 0000-0003-2779-1634.